Composites Part B 229 (2022) 109464

Contents lists available at ScienceDirect

Composites Part B

journal homepage: www.elsevier.com/locate/compositesb

Optimisation of intra-ply stitch removal for improved formability of biaxial non-crimp fabrics

S. Chen *, A.M. Joesbury, F. Yu, L.T. Harper, N.A. Warrior

Composites Research Group, Faculty of Engineering, University of Nottingham, NG7 2RD, UK

ARTICLE INFO

Keywords:
Fabrics/textiles
Defects
Finite element analysis
Forming
Resin transfer moulding (RTM)

ABSTRACT

Automated fabric forming solutions are required to meet the demand of liquid moulding processes, but wrinkling is a common problem for double-curvature parts due to a combination of the reinforcement type, manufacturing parameters and the part geometry. Local intra-ply stitch removal is introduced in the current work to improve the formability of a pillar-stitched biaxial NCF. An optimisation method is developed to remove stitches selectively, using a genetic algorithm coupled with a finite element model. Two criteria are defined to reduce the occurrence of forming defects whilst maintaining the integrity of the fabric. The first is to minimise the local shear angle across the surface of the ply and the second is to minimise the total stitch removal area. These criteria are combined into a single objective function and validated using a hemisphere forming case study. Experimental results confirm that macro-scale wrinkling can be successfully eliminated when intra-ply stitches are removed according to the optimised pattern. The stitch removal regions are distributed across both the positive and negative shear areas of the optimised NCF blank, indicating that local stitch removal can have a global effect on the formability. Perimeter shapes show that the optimum local stitch removal pattern enables a more balanced global material draw-in, demonstrating that the effect of stitch removal is not limited to the high shear regions. Removing stitches from just the over-sheared regions is therefore insufficient to fully mitigate wrinkles, justifying the need for the optimisation algorithm, as the optimised stitch removal pattern appears to be non-intuitive.

1. Introduction

Matched-tool forming is used to manufacture complex 3D fibre preforms from broad goods, including woven materials and Non-Crimp Fabrics (NCF), which are converted into fibre reinforced composite components via liquid moulding processes, such as Resin Transfer Moulding (RTM). The main challenge is to ensure preforms are free from defects, such as folds and wrinkles, as automated forming processes generally offer much less control over the local deformation of fabric plies compared to hand layup, particularly since all plies tend to be formed simultaneously.

The primary forming mechanisms for fabric plies include intra-ply shear and inter-ply slip, which occur simultaneously during automated forming of multi-ply preforms. Recent studies have focused on isolating these effects to provide greater control over preform quality. Solutions to mitigate defects during automated forming of multiple plies can be summarised into two categories. The first is to focus on improving the formability of the fabrics by modifying the fibre architecture [1], introducing inter-ply stitches for multi-ply preforms [2–4], tailoring blank shapes [5–10], introducing cuts [5] and printing localised resin patches to increase the local shear stiffness [11]. The second is to focus on modifying process parameters to manipulate the fabric forming behaviour, such as using segmented blank holders [12–16] or spring-loaded edge clamps [17–20] to modify the in-plane constraints, or using multi-piece tools [21,22] to provide greater control over material draw-in.

Non-Crimp Fabrics (NCF) typically offer increased in-plane mechanical performance compared to comparable woven fibre architectures of the same areal density [23], due to the reduced crimp of the primary yarns. Intra-ply stitches are used to consolidate the mesoscale architecture, rather than interlacing the yarns, which improves the stability of the material to prevent unwanted deformation during handling. Consequently, the formability of NCFs is generally lower, as these structural stitches restrict local shear deformation when forming complex curved components.

This paper investigates the possibility of removing local stiches from a biaxial NCF material to relax the constraints between the assembled yarns, since large shear deformation is only typically required in

* Corresponding author.
E-mail address: Shuai.Chen@nottingham.ac.uk (S. Chen).

https://doi.org/10.1016/j.compositesb.2021.109464
Received 30 June 2021; Received in revised form 2 November 2021; Accepted 4 November 2021
Available online 12 November 2021

localised regions [24]. A novel approach is presented to optimise the local stitch removal pattern of a biaxial NCF, to control the local in-plane shear deformation. A non-orthogonal constitutive model [24] is employed to simulate the forming behaviour of the plies based on a Finite Element (FE) method. An optimisation framework is presented that uses a Genetic Algorithm (GA) coupled with the FE model to remove stitches selectively, in order to minimise the occurrence of forming defects, whilst simultaneously maintaining the integrity of the fabric by minimising the stitch removal area.

2. Experimental approach

2.1. Material characterisation

FCIM359 biaxial carbon fibre non-crimp fabric (NCF), supplied by Hexcel, Leicester, UK, was used to produce all preforms in this study. The material properties are summarised in Table 1 [21]. Picture frame shear tests were performed to obtain the shear curve for the fabric material. Half of the NCF specimens were prepared with the as supplied material, while the other half of the specimens had the stitches fully removed in the central region of the picture frame. The stitches were only removed once the sample had been loaded into the picture frame rig. (See Section 2.2 for details of the stitch removal method).

The average normalised shear curves are plotted in Fig. 1. The contributions derived from the yarn rotation and the stitch stretching have been decoupled for the in-plane shear stiffness and have been expressed in the form of a polynomial (see Table 1) [24]. This enables the NCF material to be represented within the simulation either with or without intra-ply stitches. As shown in Fig. 1, the stitches significantly increase the shear resistance in the positive shear direction (shear angles >0 radians) compared to the negative direction, resulting in an asymmetric in-plane shear curve. By comparing the two shear curves it can be seen that the stitches are only active in the positive shear direction. Out-of-plane wrinkling was visibly noted at a shear angle of 43° during the picture frame tests, which is earlier than the 50° wrinkling onset angle in the negative direction (see Table 1). Local stitch removal enables more shear deformation in the corresponding region and postpones the onset of wrinkling (i.e. 55°), qualitatively indicating the potential to improve the formability and reduce manufacturing defects. However, wrinkling is not only influenced by the in-plane shear angle, but also the out-of-plane fabric bending stiffness and the in-plane tensile/compressive stiffness along the principal fibres [25–29]. It should therefore be noted that the shear angles corresponding to the onset of wrinkling were obtained based on the boundary conditions of the picture frame shear test, assuming that these values can be translated to the hemisphere forming setup.

Table 1
Material properties of FCIM359 used in non-orthogonal material model.

Material designation	FCIM359	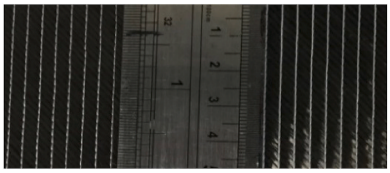
Supplier	Hexcel	
Ply thickness	0.4 mm	
Effective density	1200 kg/m^3	
Effective modulus	138 GPa	
Normalised shear curve (with stitches)	$F_{norm}^{with\ stitches} = F_{norm}^{yarn\ rotation} + F_{norm}^{stitch}$ (expressed as a function of shear angle γ_{12} in radians)	
Normalised shear curve (stitches removed)	$F_{norm}^{stitches\ removed} = F_{norm}^{yarn\ rotation}$ (expressed as a function of shear angle γ_{12} in radians)	
$F_{norm}^{yarn\ rotation}$	$(29.56\ \gamma_{12}^5 - 65.56\ \gamma_{12}^4 + 137.06\ \gamma_{12}^3 + 94.73\ \gamma_{12}^2 + 112.19\ \gamma_{12})\ N/m$	
F_{norm}^{stitch}	$\begin{cases} (2000\ \gamma_{12} - 120)\ N/m & , \ 0.06 \leq \gamma_{12} < 0.50; \\ (-3520\ \gamma_{12} + 2640)\ N/m & , \ 0.50 \leq \gamma_{12} < 0.75; \\ 0\ N/m & , \ \text{else.} \end{cases}$	
Wrinkling onset shear angle (with stitches)	Positive shear	43°
	Negative shear	50°
Wrinkling onset shear angle (stitches removed)	Positive shear	55°
	Negative shear	55°

2.2. Stitch removal

Biaxial NCF blanks (FCIM359) with dimensions 300 × 300 mm square were prepared with the 0° and 90° fibre directions aligned with the blank edges and the 45° stitch direction aligned diagonally across the blank. Full-scale stencils of the stitch removal patterns were laser-cut from cardboard and used to manually plot the patterns onto the fabric blanks. Stitches were removed by using a soldering iron to melt-sever stitches at each point of intersection between the stitch line and the plotted pattern. Each stitch line was then completely removed by unravelling the stitch chain, removing all stitching material with minimum disruption to the fibre architecture. Fig. 2 shows the quality of a typical stitch removal area that was achieved by this method.

2.3. Press tool forming

A laboratory-scale hemisphere forming tool, integrated into a universal testing machine (Instron 5581), was used for preforming the NCF, as shown in Fig. 3. Two 300 mm × 300 mm square heated platens with central holes (104 mm diameter) were used as blank holders to clamp the fabric plies. A small amount (6%wt) of reactive binder (Momentive Epikote 05390) was applied to the surface of the ply by hand, in order to create a stiff preform for post-forming analysis. The effect of the binder on the draping behaviour of the fabric was assumed negligible, since it was not heat activated prior to forming and it was used in a suitably low quantity. The effect of the binder was therefore excluded from the forming simulation.

A clamping force of 1200 N was applied to the blank holder. A hemispherical punch with a diameter of 100 mm was attached to the crosshead of the machine via a 50 kN load cell, which allowed the forming force to be monitored. A punch speed of 100 mm/min was used to form the plies. Each forming experiment was performed at ambient temperature, before the temperature of the hemispherical punch and square platens was ramped to 165 °C and held for 10 min to cure the binder. Experiments were conducted using punch displacements of 50 mm (hemisphere fully formed).

3. Optimisation methodology

3.1. Background

An optimisation method is required to minimise the occurrence of forming defects whilst minimising the area of stitch removal to maintain fabric integrity [30]. The majority of direct optimisation solutions for fabric forming problems have been implemented at the process level, to optimise parameters such as blank holding force etc., rather than tailoring local properties at the material level, due to the complex non-linear behaviour of fabric materials. In addition, each local area has to be considered individually, dramatically increasing the number of optimisation variables and therefore the complexity of the optimisation problem.

Indirect optimisation of the fabric forming process is typically performed by trial and error to produce defect-free solutions, which is highly inefficient and expensive [9,15]. Most of the solutions found are simply ‘feasible scenarios’ rather than the true global optimum, since this approach requires significant experience to interpret the results.

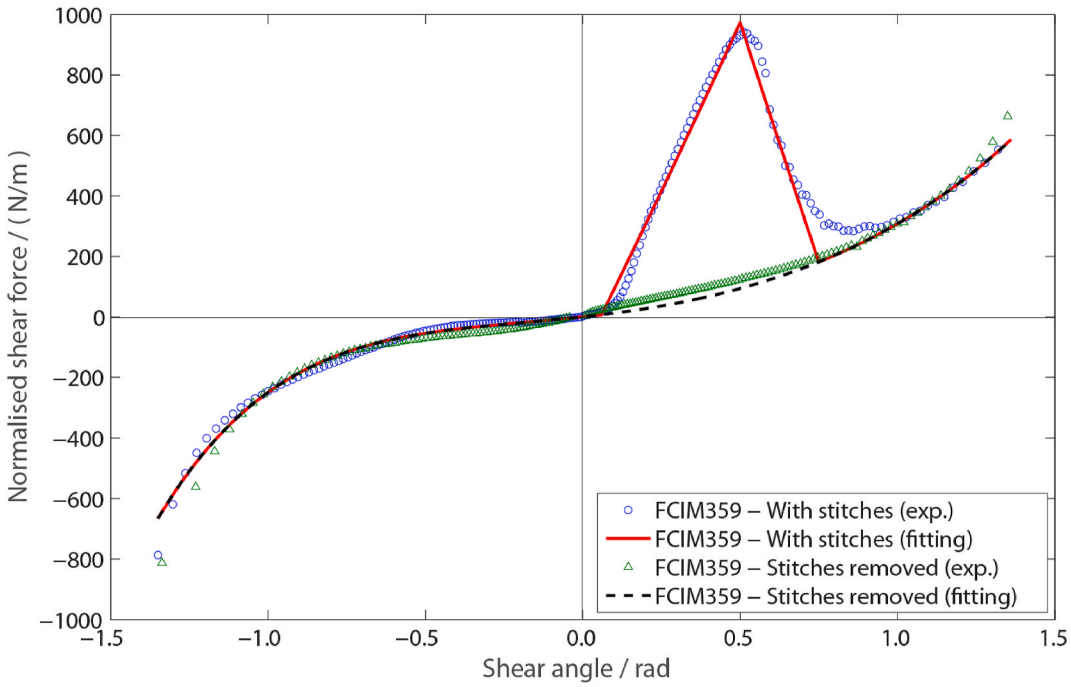

Fig. 1. Experimental picture frame shear results (average values) for FCIM359 biaxial NCF. Testing was performed in two directions, placing the stitch yarn in tension (positive shear) and compression (negative shear). Stitches were fully removed in some samples.

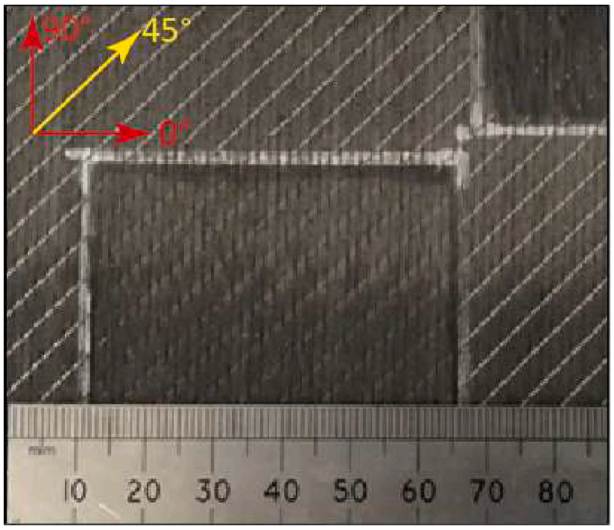

Fig. 2. Area showing stitch removal. Stitches removed with minimum disruption to the underlying fibre architecture. The first primary yarn is along the 0° direction and the second primary yarn is along the 90° direction. The intra-ply pillar stitches are along the 45° direction.

Direct optimisation methods rely on mathematical relationships to be formulated between the optimisation parameters and the objective function [17]. Gradient-based techniques are uncommon in fabric forming problems, since it is difficult to develop an objective function and its derivatives [31]. Genetic Algorithms (GA) are more widely used, which mimic the natural selection process, as variables evolve through crossovers and mutations until convergence occurs. However, this approach requires a large population to be simulated, which is computationally expensive and relies on the efficiency of the fabric forming simulation [21]. Long et al. [16] introduced a GA to optimise the peripheral pressure applied to a segmented blank holder, reducing the wrinkling strain in magnitude by between 30% and 50%. However, a truss based Finite Element (FE) model was used to achieve acceptable efficiency, compromising the numerical precision of the solution. In previous work [2,12,17,21], the authors have employed a binary encoding scheme to formulate process variables to perform optimisation using a GA, defining two different optimisation objectives derived from the shear angle distribution in each case. A large number of FE cases (>5000 cases) have to be simulated for each optimisation, which significantly increases the computational costs. Kinematic forming models [32,33] have been employed to feed quick predictions of different forming scenarios to GAs for fitness scoring. However, kinematic models use a purely geometrical approach to compute fabric drape patterns, overlooking the mechanical material properties or processing conditions, therefore only offer an approximate solution. Others have used simplified FE models using lower order elements to improve simulation efficiency [21]. Multi-step optimisation methods have also been implemented to reduce the number of optimisation variables in subsequent steps [17,21], with Artificial Neural Network (ANN) used more recently [19,34,35] using corresponding surrogate models to efficiently predict forming behaviour [19,36]. However, these both require a significant number of training cases to improve the precision of the response [29].

A FE model has been selected over a kinematic approach in this study to simulate the forming behaviour of the asymmetric biaxial NCF. The FE model has been coupled with a GA to optimise intra-ply stitch removal. Whilst a GA typically requires a large number of simulations, it provides a straightforward way to formulate the physical problem of stitch removal into a mathematical expression using an encoding scheme, and to manipulate the evolution of the stitch removal pattern automatically towards the optimum design.

The FE approach is generally slower than the kinematic approach, but there is potential to improve the efficiency of the FE model by using lower order membrane elements. Whilst this may not precisely determine the shape of wrinkles, it will be sufficient to determine their location [37] and therefore provide a fitness score for the GA. Each potential site for stitch removal corresponds to a binary number (i.e. either 0 or 1), which provides room for refining the encoding scheme to considerably reduce the number of optimisation variables, in order to

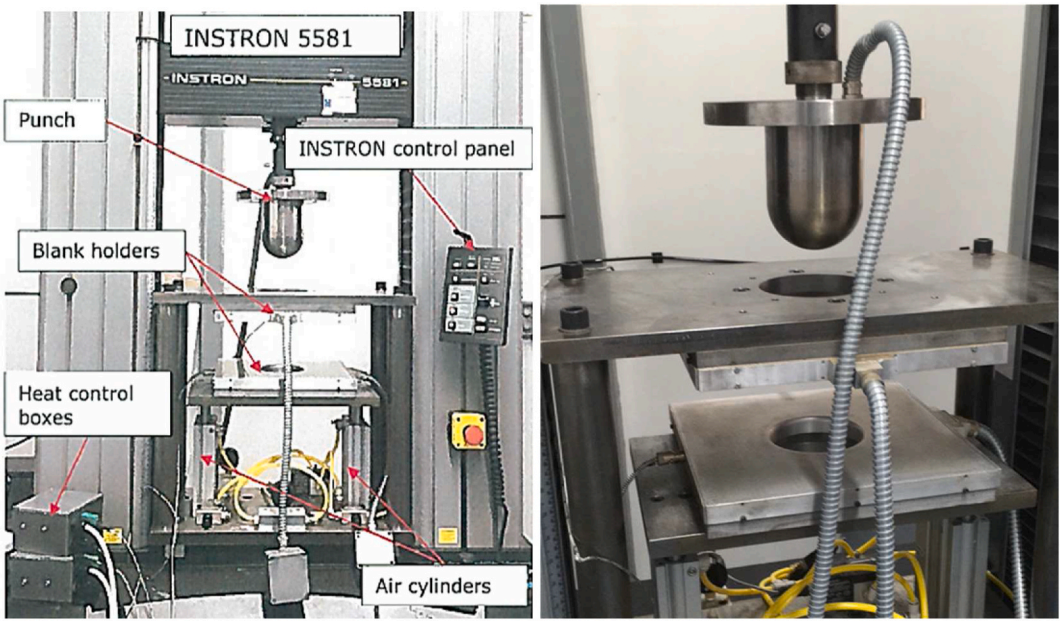

Fig. 3. Laboratory-scale hemisphere forming rig.

achieve a higher efficiency. The methodology is outlined in detail in the following section.

3.2. FE model

A FE model was developed to simulate the press tool forming process in Abaqus/Explicit, providing results to the GA for fitness scoring. All parts of the hemisphere tooling were modelled as rigid bodies, including the punch, the die and the blank holder. Only one NCF ply was formed in each case and the dimensions of each blank were 300 mm × 300 mm. Each ply was placed so that primary yarns (0°/90°) were parallel to the edge of the blank holder, with the intra-ply pillar stitches along the diagonal of the blank holder (i.e. 45°). A hypo-elastic, non-orthogonal constitutive model previously developed by the authors [24] was employed to replicate the fabric behaviour as shown in Appendix A. A user-defined subroutine (VUMAT) was developed to implement the constitutive material model in Abaqus/Explicit using the property data listed in Table 1. Two separate shear curves were implemented on an element-by-element basis, according to whether stitches had been removed or not. Square membrane elements (M3D4R) were employed to model the fabric plies, using a mesh size of 5 mm × 5 mm, which was previously confirmed to be suitable based on a mesh sensitivity study [24].

The bending stiffness of the fabric was neglected in this material model, as membrane elements were adopted, therefore it was not possible to predict the location and shape of the wrinkling defects explicitly. The global blank holder constrains the material to prevent out of plane deformation due to bending. The formability of the material is dominated by in-plane shear deformation, therefore the application of the constitutive model using membrane elements is assumed to be a reasonable compromise to improve the efficiency of the optimisation.

The contact behaviour was defined using a penalty contact algorithm. The interface friction was assumed to be isotropic using a Coulomb friction model. The tooling-fabric and fabric-fabric friction coefficients were measured to be 0.23 and 0.36 respectively, according to ASTM D1894, ISO8295. A 50 mm stroke was exerted on the punch through a displacement boundary condition, while a force varying from 1200 N to 600 N was applied to the blank holder in the form of a smooth step, which was measured as a function of the punch displacement from experiments. The displacement of the die was fully constrained.

The runtime for one forming simulation was approximately 90–180 s using an Intel® Core™ i7-3820 CPU at 3.60 GHz, which was acceptable for running the genetic algorithm to optimise intra-ply stitch removal.

3.3. Refined encoding scheme

A Genetic Algorithm (GA) was employed to optimise the stitch removal pattern, which was coupled with the FE model. An appropriate encoding scheme (see Fig. 4) was developed to implement the optimisation, to translate the stitch removal pattern into a mathematical relationship.

The whole blank area (300 mm × 300 mm) was discretised into 10 mm × 10 mm square regions (equivalent to 2 × 2 finite elements per region) prior to forming. Each region represents a potential stitch removal site corresponding to a binary bit, where a value of unity denotes “stitches removed”, while zero denotes “stitches remain”. The stitch removal pattern was formulated using a binary encoding scheme as shown in Fig. 4, representing a binomial-status series. This digitised expression facilitates GA manipulations to perform a heuristic search for the optimum stitch removal pattern, which can be written as

$$s = \overline{p_1 \;\; p_2 \;\; \cdots \;\; p_{i-1} \;\; p_i \;\; p_{i+1} \;\; \cdots \;\; p_n} \tag{1}$$

where s represents the stitch removal pattern;

$$p_i = \begin{cases} 1, & \text{stitches removed;} \\ 0, & \text{stitches remain.} \end{cases} \quad (i = 1,\ 2,\ \cdots,\ n) \tag{2}$$

denotes the status of stitch removal at the ith location, which represents the stitch removal status for 4 finite elements in the corresponding 10 mm × 10 mm square; where n denotes the total number of potential locations.

For each loop of the algorithm (one generation), a group of stitch removal patterns is generated, which are effectively “individuals” in the binary series. If each binary bit (i.e. p_i) was considered to be a variable, the number of optimisation variables would be 900, which would be impractical to implement. Due to the symmetry of the blank with respect to the two diagonals, the number of bits in the binary series can be reduced to 240 (i.e. $n = 240$), but this is still impractical. Thus, this series was divided into short segments as shown in Fig. 4, where each segment was considered as an optimisation variable (i.e. v_j) including several binary bits. Consequently, the number of variables is

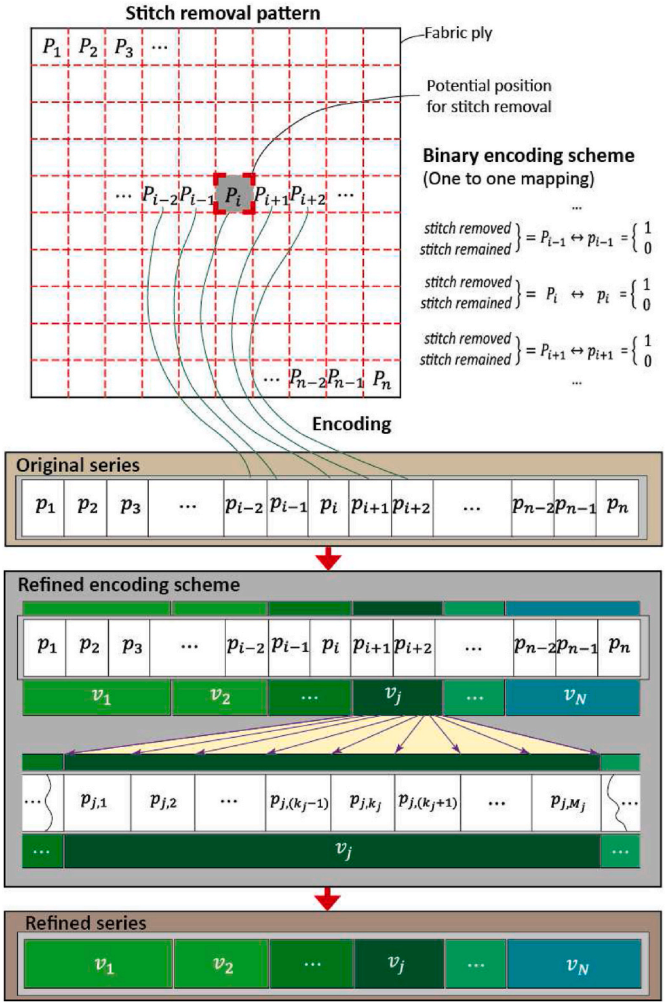

Fig. 4. Refined encoding scheme to formulate stitch removal pattern, based on the basic binary encoding scheme in Ref. [2].

dramatically reduced to 16, enabling the optimisation routine to be effectively implemented. The numerical expression for the stitch removal pattern can be refined to be

$$s = \overline{v_1 \;\; v_2 \;\; \cdots \;\; v_{j-1} \;\; v_j \;\; v_{j+1} \;\; \cdots \;\; v_N} \tag{3}$$

where

$$v_j = \overline{p_{j,1} \;\; p_{j,2} \;\; \cdots \;\; p_{j,(k_j-1)} \;\; p_{j,k_j} \;\; p_{j,(k_j+1)} \;\; \cdots \;\; p_{j,M_j}} \quad (j = 1, \;\; 2, \;\; \cdots, \;\; N) \tag{4}$$

denotes the jth optimisation variable; N denotes the number of optimisation variables in total; M_j denotes the number of bits in the jth optimisation variable; p_{j,k_j} denotes the k_j^{th} bit in the jth optimisation variable

$$p_{j,k_j} = \begin{cases} 1, & \text{stitches removed;} \\ 0, & \text{stitches remained.} \end{cases} \quad \left(j = 1, \;\; 2, \;\; \cdots, \;\; N; \;\; k_j = 1, \;\; 2, \;\; \cdots, \;\; M_j\right) \tag{5}$$

and

$$n = \sum_{j=1}^{N} M_j \tag{6}$$

Each segment was considered as an optimisation variable, including 15 bits i.e. $M_j = 15 \;\; (j = 1, 2, \cdots, 16)$. Consequently, only 16 variables (i.e. $N = 16$) were used to implement the optimisation routine.

Each variable in the refined encoding scheme includes more than one binary bit and each bit denotes an independent stitch removal region. Thus, the number of optimisation variables is significantly reduced, as the variables in the refined encoding scheme carries more information than the original binary encoding scheme [2]. This reduces the overall population size in the GA, whilst ensuring sufficient diversity.

3.4. Optimisation of stitch removal pattern

Two different optimisation criteria, maximum value criterion (MAXVC) and Weibull distribution quantile criterion (WBLQC), were previously developed by the authors [2] as GA fitness functions to quantitatively assess fabric forming quality. However, they were both designed for a material continuum with consistent material behaviour over the entire area. Due to the removal of stitches, the shear behaviour changes locally within the blank, therefore establishing the defect status of these dissimilar areas is more difficult, as out-of-plane wrinkling is postponed until a shear angle of 55° in the stitch removal area (compared to 43° in positive shear and 50° in negative shear for no stitch removal). Hence, the shear angle should be normalised in the objective function accordingly

$$\overline{\gamma_{12}} = \begin{cases} \dfrac{\gamma_{12}}{|\gamma_{12}^{+}|}, & 0^\circ \le \gamma_{12} < 90^\circ; \\ \dfrac{\gamma_{12}}{|\gamma_{12}^{-}|}, & -90^\circ < \gamma_{12} < 0^\circ. \end{cases} \tag{7}$$

where, γ_{12} is the shear angle in degree; $\overline{\gamma_{12}}$ is the normalised shear angle and $\overline{\gamma_{12}} \in \left(\frac{-90^\circ}{|\gamma_{12}^{-}|}, \;\; \frac{90^\circ}{|\gamma_{12}^{+}|}\right)$; $|\gamma_{12}^{+}|$ is the magnitude of the wrinkling onset shear angle in positive shear; $|\gamma_{12}^{-}|$ is the magnitude of the wrinkling onset shear angle in negative shear.

This normalisation provides a consistent indicator of defects for the two distinct material regions. In this case, $\overline{\gamma_{12}} \in \left(\frac{-90^\circ}{50^\circ}, \;\; \frac{90^\circ}{43^\circ}\right) = (-1.800, \; 2.093)$ when the stitches are not removed, otherwise $\overline{\gamma_{12}} \in \left(\frac{-90^\circ}{55^\circ}, \;\; \frac{90^\circ}{55^\circ}\right) = (-1.636, \; 1.636) \subset (-1.800, \; 2.093)$. Thus, $\overline{\gamma_{12}} \in (-1.800, \; 2.093)$.

The MAXVC [2] was adopted here, as it was previously shown to be an appropriate compromise between convergence speed and accuracy [17]. This objective function was used to ensure local shear angles do not exceed the fabric shear locking angle.

After normalising the shear angle, the updated objective function can be written as

$$f_{\text{MAXVC}}\{v_1, v_2, \;\; \cdots, v_N; \overline{\gamma_{12}}\} = \max_{i=1,2,\ldots,m} \{|\overline{\gamma_i}|\} \tag{8}$$

where $f_{\text{MAXVC}}\{\cdot\}$ denotes the fitness function using MAXVC, which aims to minimise the maximum normalised shear angle; m is the total number of material points; $|\cdot|$ is the absolute value of the variable; $\overline{\gamma_i}$ is the value of the normalised shear angle at the ith material point. Since the stitch removal pattern influences the normalised shear angle distribution, the value of f_{MAXVC} was used for quantitative assessment of the fitness. In this case, $f_{\text{MAXVC}} \in [0.000, \;\; 2.093)$.

As stitch removal typically leads to an increase in the wrinkling onset shear angle, total stitch removal is theoretically considered to be the optimum pattern if minimising the maximum normalised shear angle is the only objective. However, excessive stitch removal induces serious problems in practice for handling, removing all through-thickness meso-scale reinforcement. Therefore, a minimum stitch removal area must be imposed with respect to the overall area of the NCF blank, which is referred to as the Total Stitch Removal Area Criterion (TSRAC). Since the finite element size is constant for the fabric blank, the TSRAC can be expressed as

$$f_{\mathrm{TSRAC}}\{v_1, v_2, \cdots, v_N; p_k\} = \sum_{k=1}^{K} \frac{p_k}{K} \tag{9}$$

where, $f_{\mathrm{TSRAC}}\{\cdot\}$ denotes the fitness function using TSRAC, which aims to minimise the total area of stitch removal; p_k denotes the status of stitch removal at the kth element of the NCF; K is the total element number of the fabric preform. In this case, $f_{\mathrm{TSRAC}} \in [0.000,\ 1.000]$.

According to the MAXVC objective, the formability of the NCF can be optimised to mitigate forming-induced defects by minimising the value of f_{MAXVC} . The TSRAC objective can be used to control the preform integrity by minimising the stitch removal area by minimising the value of f_{TSRAC}. However, defect mitigation takes priority over reducing the total area of stitch removal in this optimisation, so once all defects are suppressed, the focus is shifted to minimising the area for stitch removal. These two objectives can therefore be combined into a single objective for stitch removal optimisation ($f\{v_1, v_2, \cdots, v_N\}$), which can be written as

$$f\{v_1, v_2, \cdots, v_N; \overline{\gamma_{12}}, p_k\} = \begin{cases} f_{\mathrm{MAXVC}} - 1, & \text{defect;} \\ f_{\mathrm{TSRAC}} - 1, & \text{defect} - \text{free.} \end{cases} \tag{10a}$$

or

$$f\{v_1, v_2, \cdots, v_N; \overline{\gamma_{12}}, p_k\} = \begin{cases} \max\limits_{i=1,2,\ldots,m} \{|\overline{\gamma_i}|\} - 1, \max\limits_{i=1,2,\ldots,m} \{|\overline{\gamma_i}|\} - 1 > 0; \\ \left(\sum\limits_{k=1}^{K} \frac{p_k}{K}\right) - 1, \max\limits_{i=1,2,\ldots,m} \{|\overline{\gamma_i}|\} - 1 \le 0. \end{cases} \tag{10b}$$

In this case, when the preform is defect-free, $f \in [-1.000,\ 0.000]$; otherwise, $f \in (0.000,\ 1.093)$.

Therefore, the multi-objective optimisation problem for stitch removal is converted to a single-objective optimisation problem, which can be written as

$$\text{minimise } f\{v_1, v_2, \cdots, v_N; \overline{\gamma_{12}}, p_k\} \quad \text{subject to} \begin{cases} v_j \in \text{Integer } (j = 1, 2, \ldots, N) \\ v_j \in [0,\ 2^{M_j}]\ (j = 1, 2, \ldots, N) \\ \gamma_{12} \in (-90°, 90°) \end{cases} \tag{11}$$

This optimisation is expected to minimise the occurrence of wrinkling by effectively removing local stitches. The primary objective is to eliminate wrinkles, with a second objective to minimise the stitch removal area triggered once the preform is confirmed to be defect-free.

3.5. Optimisation implementation

As shown in Fig. 5, a script was developed for stitch removal optimisation using the GA Toolbox in Matlab, which was integrated with the FE simulation to submit new Abaqus jobs and evaluate results for fitness assessment. The workflow of the Matlab GA Toolbx is shown in Appendix B. For each loop or "generation" in the GA, a group of stitch removal patterns called "individuals" was generated according to the refined encoding scheme. Each series was interpreted to update the material definition (either with stitches present or removed) for the corresponding input file, which was submitted to Abaqus/Explicit. An FE analysis was conducted for each individual, with shear angles returned to Matlab. The defined objective function was invoked to determine the corresponding fitness value to check for convergence. The iteration loop continued unless the optimum was achieved. The optimisation process took 113.5 h for the hemisphere geometry studied in the current work, using 4 CPUs in total.

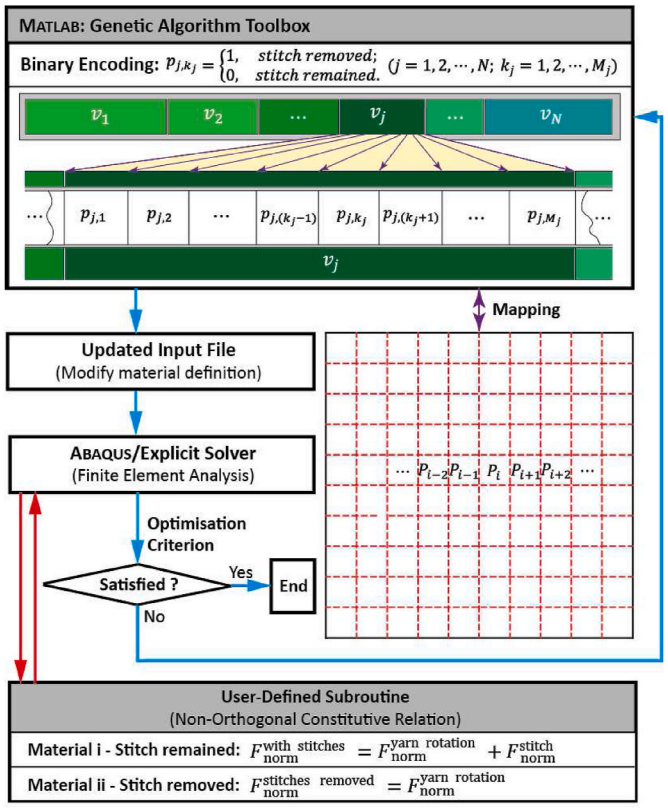

Fig. 5. Implementation of localised stitch removal optimisation.

4. Results and discussion

4.1. Implementation of objective function

The optimisation was performed according to the flowchart shown in Fig. 5, with 16 optimisation variables, using the refined encoding scheme in Section 3.3. The stability of a GA for delivering an optimum solution depends on the diversity of the population, which is determined by the initial chosen population, the population size, and probabilities for crossover and mutation [17]. For this GA, a population size of 100 was chosen to be greater than twice the total number of variables in the optimisation. The initial population was generated randomly to ensure sufficient diversity, while the probabilities of the crossover and mutation were determined adaptively, based on the fitness scores from the previous generation.

As shown in Fig. 6, the fitness score gradually decreases during the optimisation and finally converges to its minimum, i.e. −0.7022, after the 42nd generation. Since a negative fitness score is achieved at the optimum, the corresponding maximum shear angle should be less than the wrinkling onset value (i.e. $f_{\mathrm{MAXVC}} - 1 \le 0$) and the value of ($f_{\mathrm{TSRAC}} - 1$) is assigned to the fitness score according to the definition of the combined fitness function. Thus, a stitch removal pattern has been obtained from the optimisation to produce a defect-free preform and the corresponding minimum total stitch removal area is 29.78%. From the 8th generation, individuals with negative fitness scores were first created during the evolution of the GA (see the best fitness in Fig. 6). This implies that at least one stitch removal pattern (i.e. one individual)

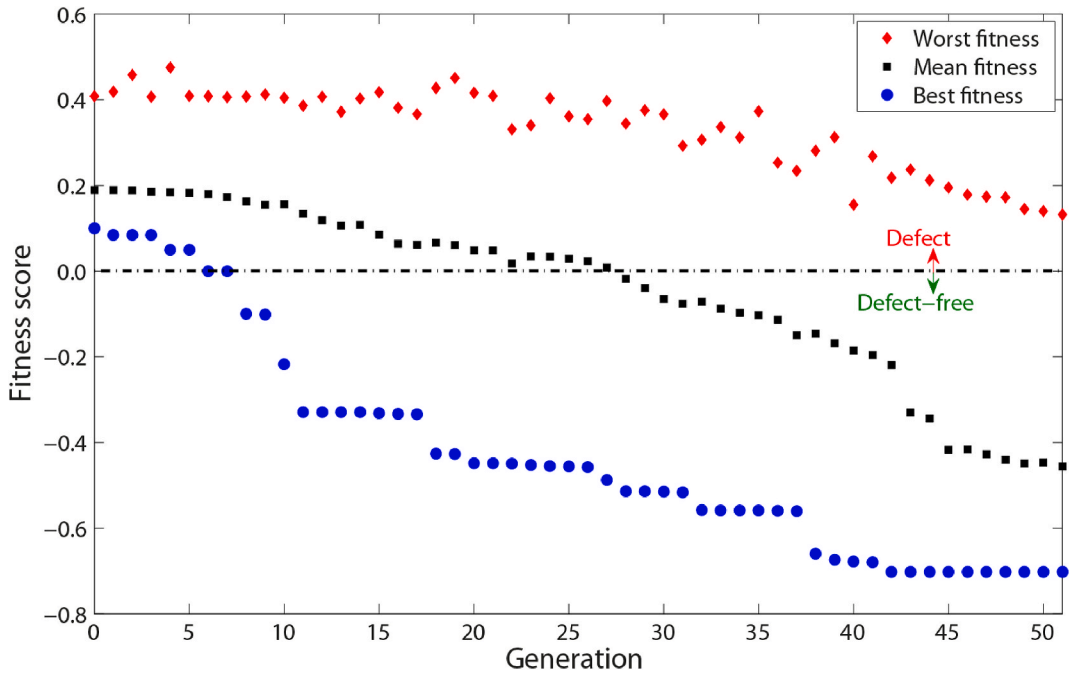

Fig. 6. Evolution of the fitness score in the intra-ply stitch removal optimisation for a 0°/90° NCF with 45° pillar stitches.

from the GA population has yielded a defect-free preform since the 8th generation. The optimum is achieved from the 42nd generation and perturbations induced by further mutations in the GA during the next 10 generations appear to have no influence on the optimum solution. Therefore, Fig. 6 confirms that the present level of diversity prevents local optimum solutions, random selection and instability.

Each individual in the optimisation corresponds to a pair of f_{MAXVC} and f_{TSRAC} values, which are used to determine the fitness score. Thus, these values can be used as the (x, y) coordinates to determine a point of (f_{MAXVC}, f_{TSRAC}) in a 2D space representing an individual in the GA population. All of the individuals are plotted as a point cloud in blue in Fig. 7. The line of $f_{\mathrm{MAXVC}} = 1$ (see the vertical black dashed line in Fig. 7) divides the solution space into two parts, creating a defect-free region on the left and a defective region on the right. The Pareto front (purple line in Fig. 7) indicates a set of solutions that are all independent to each other, but are superior to the rest of the population for this multi-objective problem. The optimum solution should therefore be selected from the Pareto front in the defect-free region and with the minimum value of f_{TSRAC}, which is highlighted by a green circle in Fig. 7 (Point (0.9971, 0.2978)) for the current problem. This is consistent with the optimum determined using the combined objective function defined in Section 3.4. Results show that the conversion from multi-objective to single-objective optimisation for stitch removal can reasonably determine the optimal solution by converging in the correct direction, i.e. minimising the stitch removal area with no occurrence of wrinkles. The MAXVC criterion essentially serves as a filter to sift for defect-free solutions before applying the TSRAC criterion.

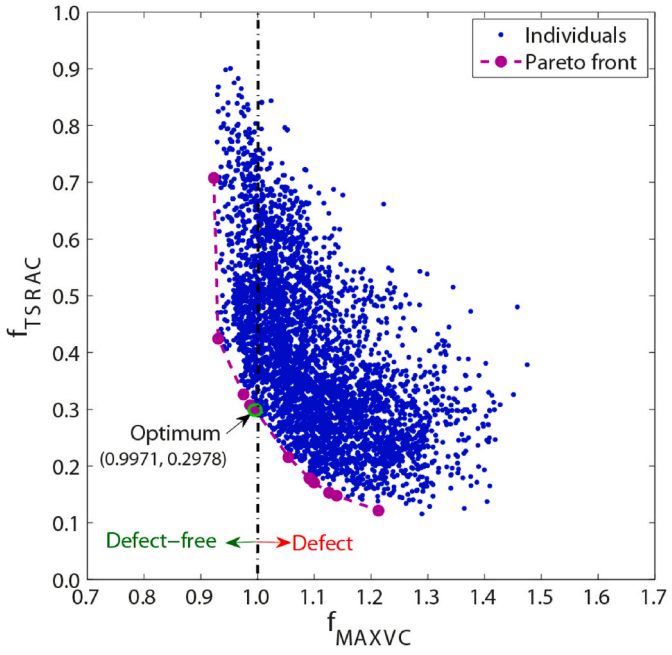

Fig. 7. Pareto front of the stitch removal optimisation.

As shown in Fig. 8, the combined objective function is able to distinguish the defect-free individuals from the rest of the GA population without any overlaps. As a unit offset was applied to both f_{MAXVC} and f_{TSRAC} to form the combined fitness function, it prevents any overlap between the two sub-populations. These results indicate that the objective can successfully be switched in the stitch removal optimisation from MAXVC (i.e. minimising defects) to TSRAC (i.e. minimising removal area).

The minimum value of f_{MAXVC} decreases significantly until the first defect-free solution ($f_{\mathrm{MAXVC}} \leq 1.0$) is found at the 8th generation (see the blue dashed line in Fig. 9), where it overlaps with one from the defect-free subpopulation (see the blue solid line in Fig. 9) and continues to fluctuate around ~0.95 for subsequent generations. This implies that the dominant optimisation objective is to minimise the maximum shear angle (MAXVC), which then switches to the other objective among the defect-free subpopulation to produce the optimum.

As shown in Fig. 10, the overall stitch removal area (i.e. the normalised sum of the optimisation variables) is selected from a wide range (i.e. from ~0.1 to 0.9), indicating an appropriate diversity of the GA population. There are overlaps between the defect-free and defective subpopulations, so it is essential to distinguish them using MAXVC prior to determining the optimum. According to Fig. 7, (f_{MAXVC}, f_{TSRAC}) is equal to (0.9971, 0.2978) at the optimum. The converged minimum value of f_{TSRAC} in Fig. 10 does not correspond to the minimum value of f_{MAXVC} (i.e. ~0.92 as shown in Fig. 9). Thus, the optimum solution is a

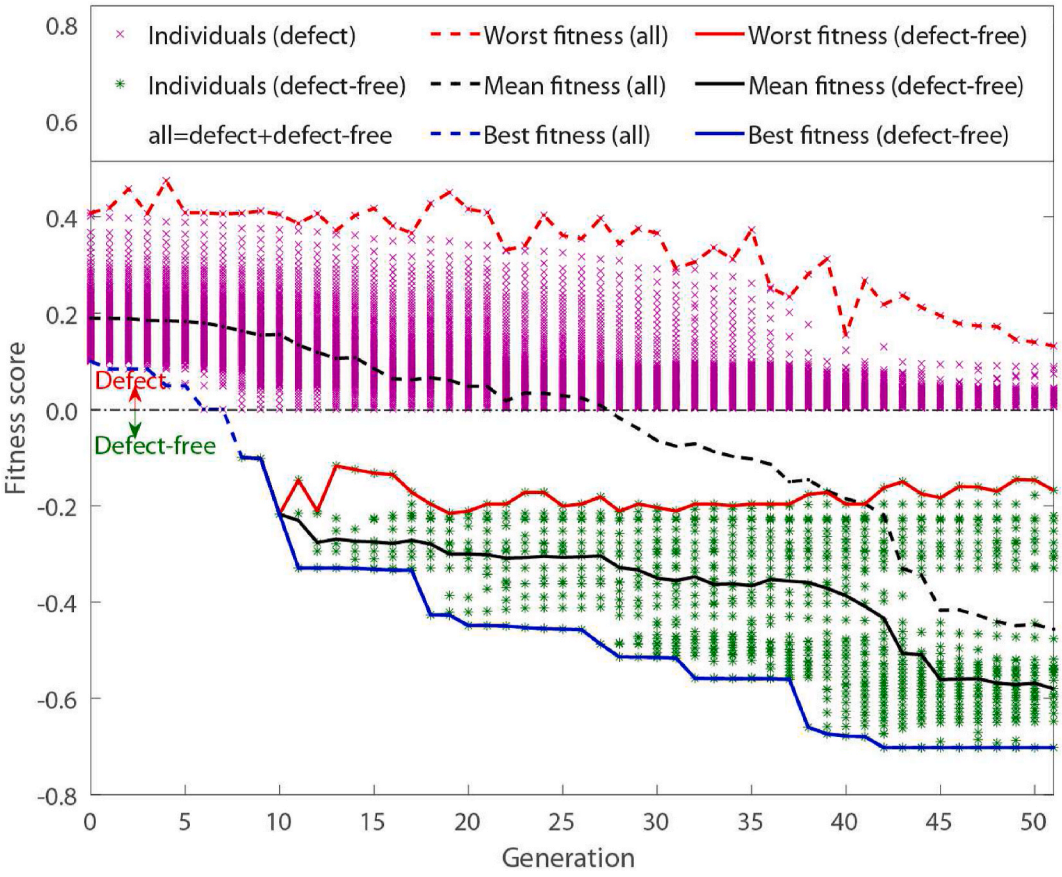

Fig. 8. Comparison of the fitness score evolutions among the entire GA population and the defect-free subpopulation.

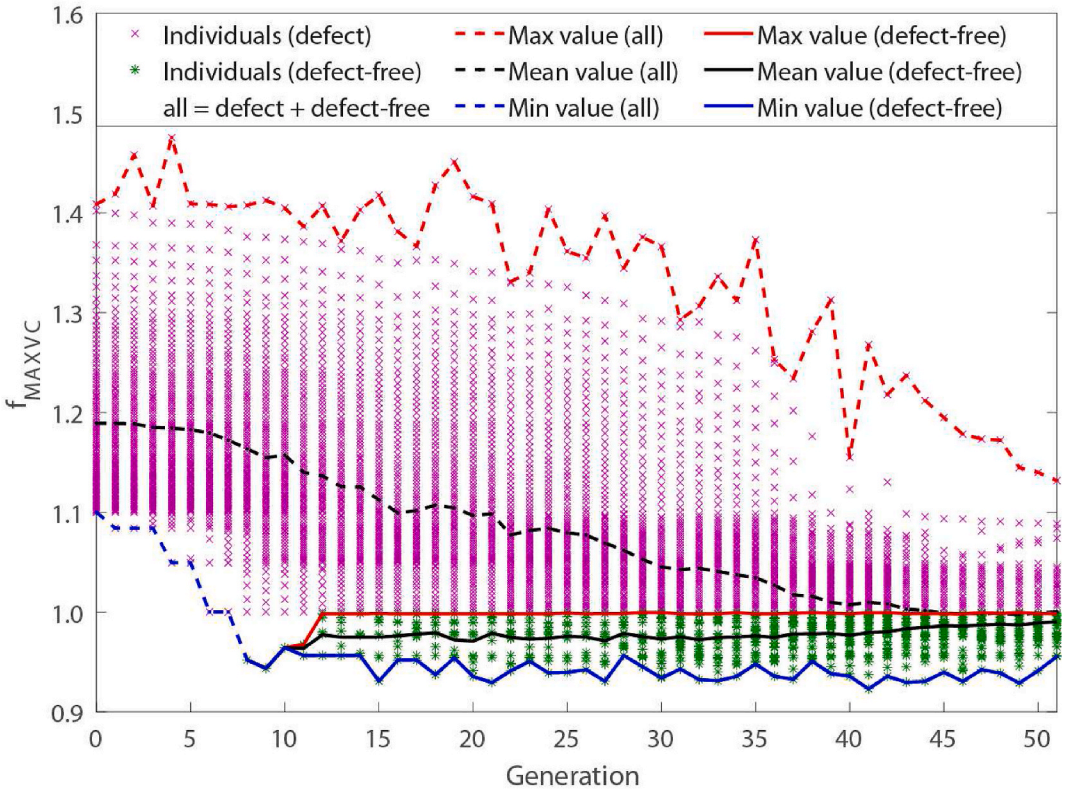

Fig. 9. Comparison of the MAXVC evolutions among the entire GA population and the defect-free subpopulation.

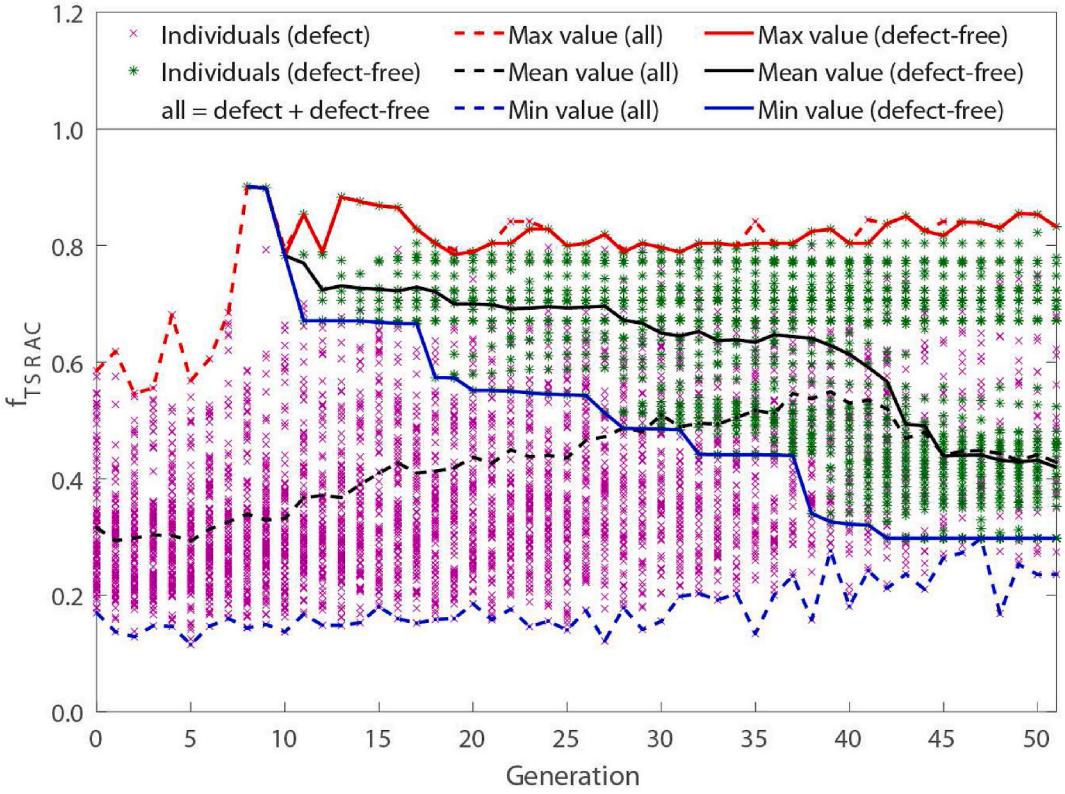

Fig. 10. Comparison of the TSRAC value evolutions among the entire GA population and the defect-free subpopulation.

compromise between minimising the occurrence of defects and minimising the stitch removal area, but these two objectives may not be achieved simultaneously.

4.2. Optimum stitch removal pattern

The optimum intra-ply stitch removal pattern was determined from the optimisation as shown in Fig. 11. The red elements in Fig. 11(a) require stitch removal, while the stitches in the blue elements should remain. The stitch removal regions are distributed across both the positive and negative shear areas to ensure there is a change in the global forming response of the blank. A blank was created using the optimised pattern, as shown in Fig. 11(b), which was formed using the hemisphere press tool.

4.2.1. Influence on wrinkle formation

As shown in Fig. 12 and Fig. 13, the resulting formed shape was compared against the reference case (i.e. no stitch removal). The images

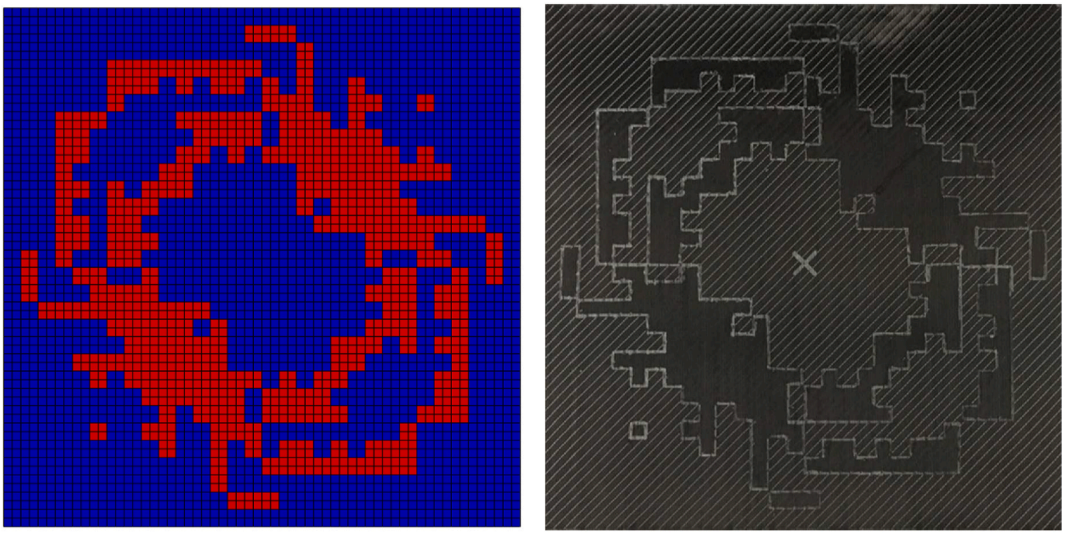

Fig. 11. Optimum pattern for intra-ply stitch removal from a 0°/90° NCF with pillar stitches along +45° direction. The red regions denote the stitch removal regions in the optimum pattern, while the blues regions denote the regions without intra-ply stitch removal.
(a) Optimum pattern (b) Experiment

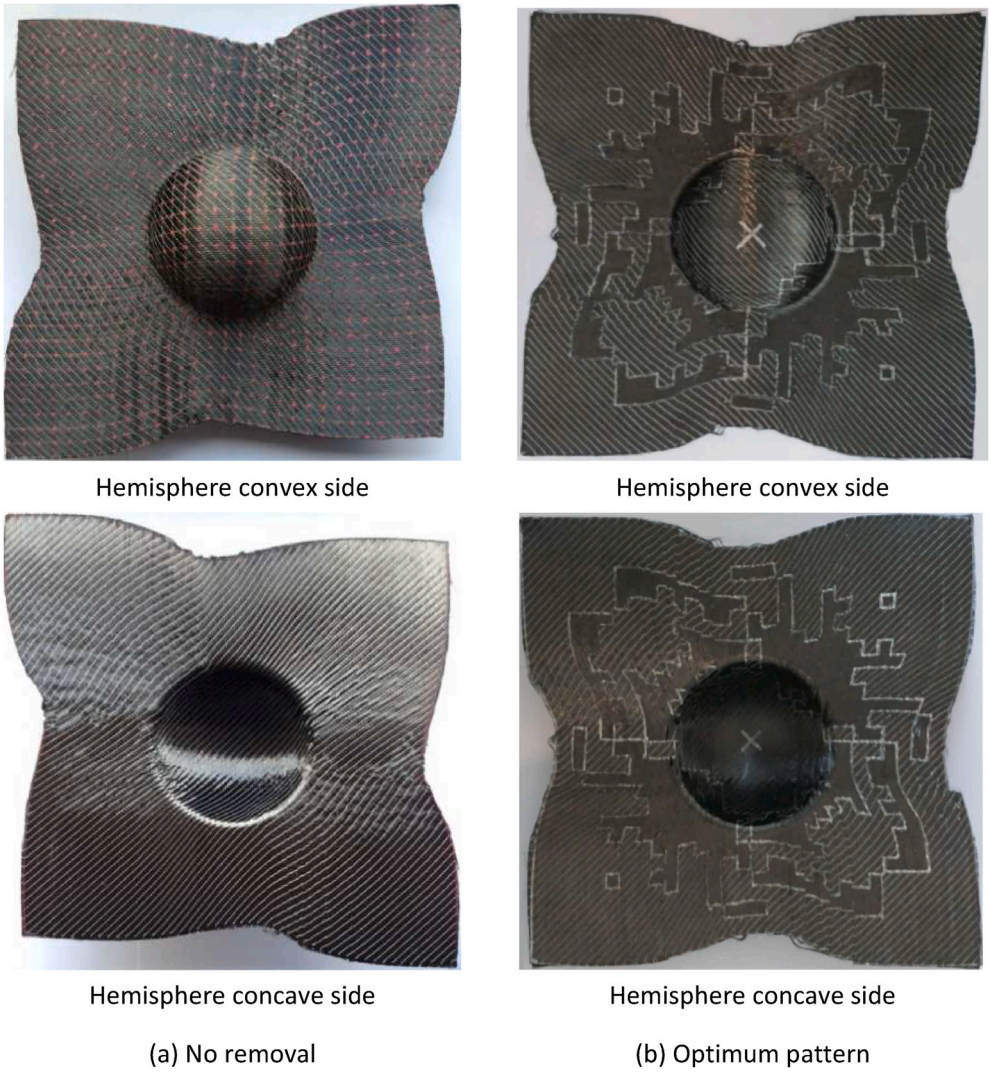

Fig. 12. Comparison of the produced preform using the optimum stitch removal pattern against the baseline without stitch removal. (a) No removal (b) Optimum pattern

confirm that macro-scale wrinkling is successfully eliminated when the intra-ply stitches are removed according to the optimised pattern, with sufficient stitch integrity remaining in the meso-scale fibre architecture to prevent the preform from falling apart. As shown in Fig. 13(a), the preform surface of the reference case is uneven due to out-of-plane wrinkles, which influence the mechanical efficiency of the primary yarns (due to fibre buckling). Macro-scale wrinkles occur within the positive shear regions in the form of out-of-plane waviness, while meso-scale in-plane wrinkles mainly occur in negative shear regions due to constraints from the blank holder.

By removing stitches according to the optimum pattern, both macro-scale and meso-scale wrinkling is significantly reduced, as shown in Fig. 13(b). The removal of stitches relaxes any constraints on yarn rotation, improving the formability of the NCF and therefore eliminating wrinkles. As the removal area is minimised in the optimisation, the application of the optimum pattern does not result in other considerable defects, such as laddering or intra-ply yarn sliding. However, Fig. 13(b) indicates some small areas of fibre/ply splitting on the surface among the stitch removal regions, due to shear deformation. This potentially creates gaps or channels in the surface of the NCF, which may cause resin-rich regions in the cured composite component and consequently a reduction in local mechanical properties. These gaps are also likely to influence the local permeability of the preform and therefore process repeatability.

These ply splitting effects are localised and do not occur in all regions of stitch removal. Whilst the total area of stitch removal was minimised during the optimisation to reduce adverse effects on the material integrity, additional constraints may be required to eliminate these additional side effects. For example, a limit may be required on the size of each local stitch removal area, or restrictions may need to be imposed on the location of stitch removal according to the relative orientation of the primary yarns.

Results indicate that the developed method for stitch removal optimisation is able to determine a feasible solution to produce wrinkle-free NCF preforms by simultaneously considering two objectives: minimising the wrinkling onset angle and minimising the stitch removal area. The risk of destroying the meso-scale architecture by excessive stitch removal was only considered implicitly by means of minimising the overall removal area. A more comprehensive defect criterion could be developed to replace the MAXVC to improve optimisation performance.

4.2.2. *Influence on shear angle distribution*

The normalised shear angle was defined in Section 3.4 as an appropriate indicator to identify wrinkling defects in different material regions. The distribution of the normalised shear angle is compared in Fig. 14 for the baseline and the optimum case. Wrinkling typically

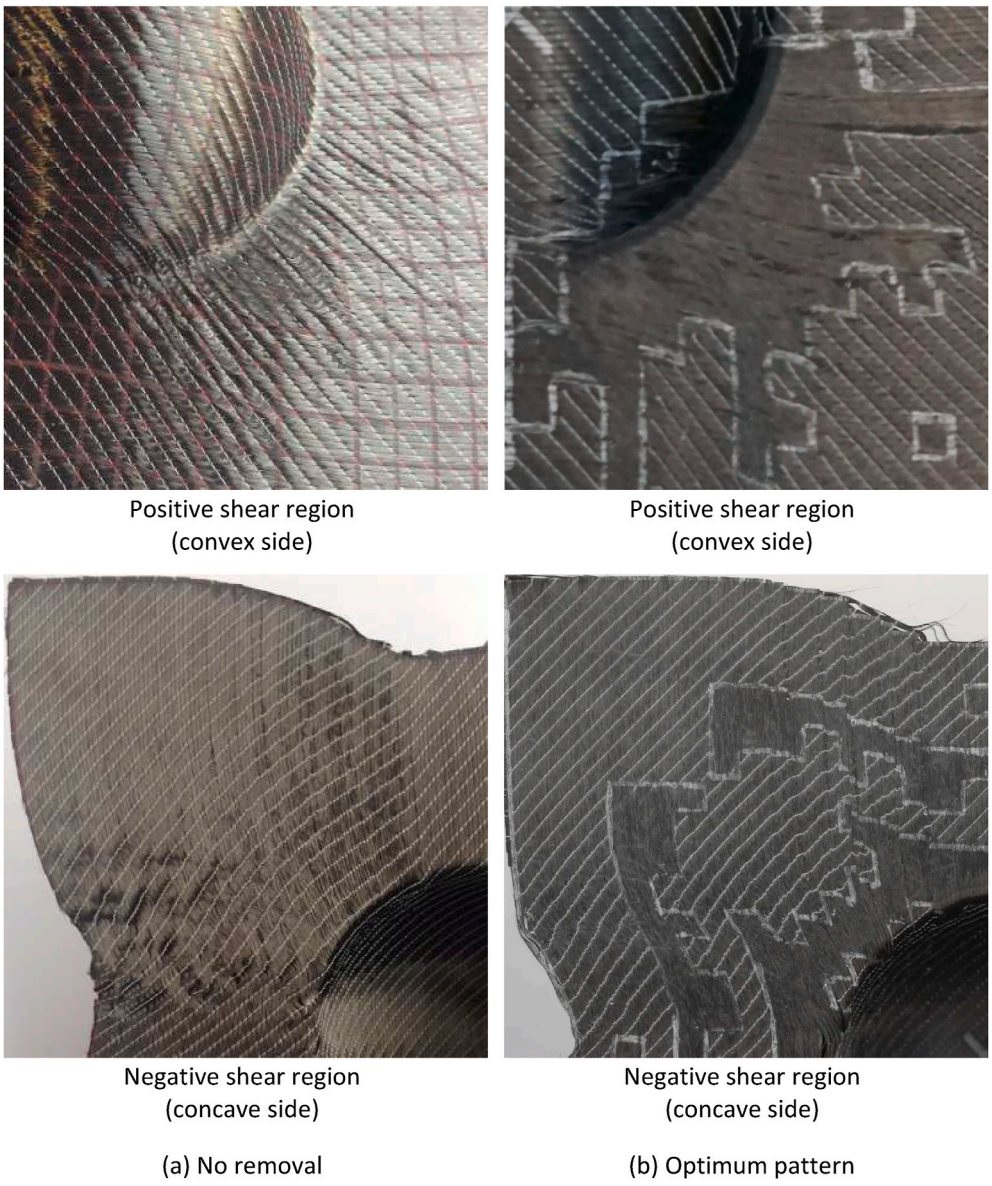

Fig. 13. Comparison of detailed defects between the preform using the optimum stitch removal pattern and the baseline (without stitch removal). (a) No removal (b) Optimum pattern

occurs when the magnitude of the normalised shear angle (i.e. the absolute value) is greater than 1.00. In this hemisphere forming process, stitch removal results in a significant reduction in normalised shear angle by using the optimum pattern (see Fig. 14(b)) with respect to the baseline (see Fig. 14(a)). The magnitude of the normalised shear angle decreases to less than 1.00 (maximum 0.9971) by adopting the optimised stitch removal pattern. This implies that the occurrence of wrinkles is eliminated by the optimisation process, supporting the observations in Figs. 12 and 13.

For the optimum pattern, the total stitch removal area is 29.78% of the total blank area, which is the minimum area shown to completely mitigate wrinkles. This pattern is overlaid on top of the normalised shear angle distribution of the baseline in Fig. 15 to investigate the distribution of the stitch removal areas compared to the distribution of the high shear regions. As shown in Fig. 15, the stitch removal areas are coincident with the largest over-sheared regions (i.e. the magnitude of the normalised shear angle larger than 1.00 in light grey). All light grey regions of wrinkling are contained within Fig. 15(a), with no wrinkle areas visible in Fig. 15(b). The removal of intra-ply stitches in these areas relaxes the local constraints and enables greater rotation of the yarns. However, a large percentage of the stitch removal area (~80%) from the optimum pattern is outside of these excessively sheared regions of the original NCF ply. Whilst the implementation of stitch removal is local, its effect is not limited to the corresponding regions of high shear. The formability of material in nearby regions must be changed accordingly to relieve defects caused by over-shearing. Results indicate that simply removing stitches from the defective regions may not be sufficient to fully mitigate wrinkles.

4.2.3. *Influence on material draw-in*

Material draw-in is typically measured from the change in the perimeter shape of the preform, which is an overall indicator of material deformation during forming. The perimeter shapes are compared between the simulation and the experiment for the reference and the optimal case, as shown in Fig. 16. The Root Mean Square Error (RMSE) of the predicted perimeter for the baseline case (see Fig. 16(a)) is calculated to be 2.07%, while the RMSE for the optimal case is 3.84%. The simulation shows good agreement with the experiment for the stitch

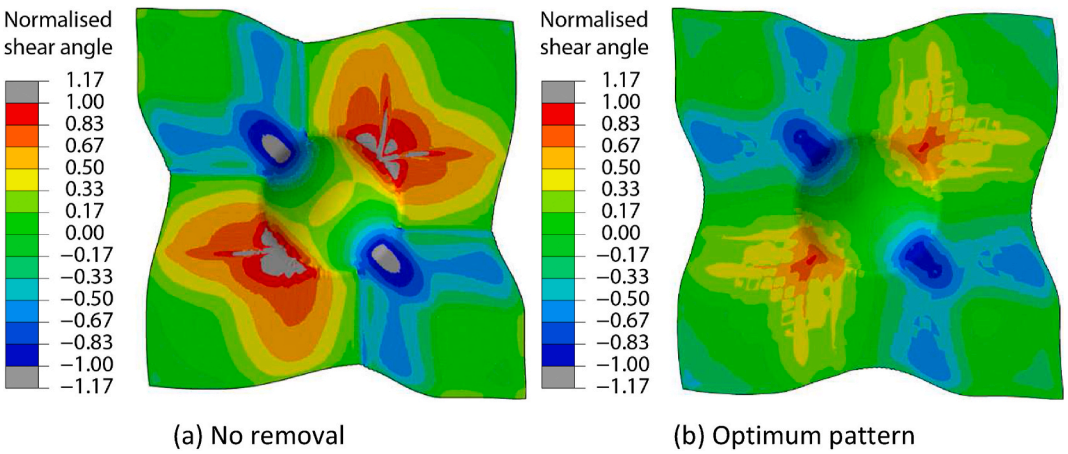

Fig. 14. Comparison of normalised shear angle distribution from simulation. A normalised shear angle >1 or <-1 (light grey) indicates local area of wrinkling. The punch stroke is 50 mm and 75% interpolation smoothing is used for the contours.
(a) No removal (b) Optimum pattern

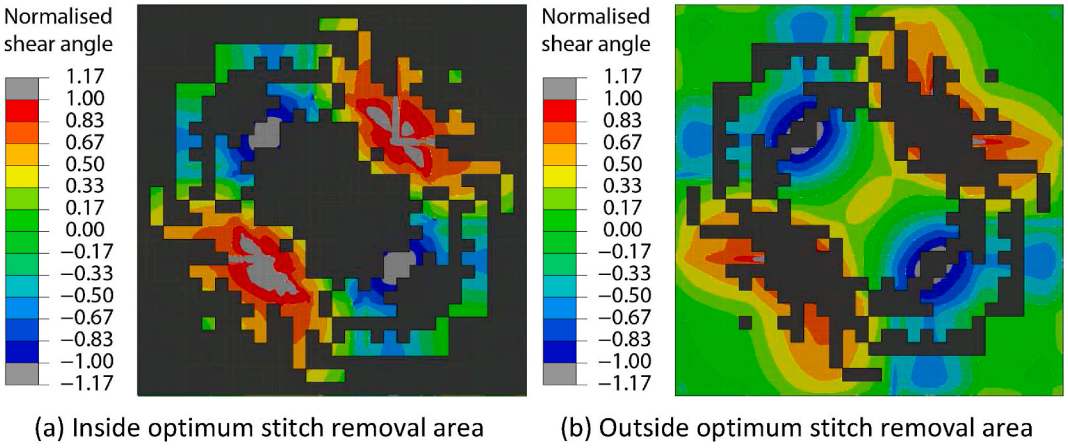

Fig. 15. Optimum stitch removal pattern overlaid on top of normalised shear angle distribution of the undeformed blank without stitch removal. A normalised shear angle >1 or <-1 (see light grey areas according to legend) indicates local areas of wrinkling.
(a) Inside optimum stitch removal area (b) Outside optimum stitch removal area

removal case, indicating that the binary approach to modelling the NCF material with and without stitches is valid. According to Fig. 16, the difference between the two diagonals is 33 mm for the baseline case and just 8 mm for the optimum stitch removal pattern. This observation, plus the change in perimeter shape, confirms that the optimum stitch removal pattern has successfully reduced the asymmetry of the biaxial NCF in comparison to the baseline case. This indicates that the optimum local stitch removal pattern produces a more balanced global material draw-in profile.

5. Conclusions

Local intra-ply stitch removal was introduced to improve the formability of a biaxial NCF with a pillar stitch pattern. An optimisation method was developed using a genetic algorithm coupled with a finite element model to remove stitches selectively, in order to minimise the occurrence of forming defects whilst simultaneously minimising the total area of stitch removal. This optimisation method was employed to determine an optimum stitch removal pattern for a hemispherical component produced by a press tool forming process. Experimental results confirmed that macro-scale wrinkling is successfully eliminated when the intra-ply stitches are removed according to the optimised pattern, and there is sufficient stitch integrity remaining in the meso-scale fibre architecture to prevent the preform from falling apart. Some small areas of fibre/ply splitting were observed on the surface of the preform among the stitch removal regions, despite the total stitch removal area being minimised. Further constraints may be required to eliminate these side effects, such as controlling the size of the local stitch removal area.

The stitch removal regions in the optimum pattern are distributed across both the positive and negative shear areas, indicating that local stitch removal could have a global effect on the formability, but the removal pattern is a compromise between the shear performance and the preform integrity. The effect of stitch removal does not appear to be limited to just the corresponding regions of high shear, and therefore simply removing stitches from the defective regions may not be sufficient to fully mitigate wrinkles. The change in perimeter shape shows that the optimum local stitch removal pattern produces a more global balanced material draw-in profile, reducing the asymmetry of the fabric. This demonstrates that the global shear compliance of the biaxial NCF ply in the positive direction is now similar to the shear compliance in the negative direction.

In practice, stitch removal could be implemented by laser ablation or another carefully controlled heat source located on a gantry robot, offering the potential to automate the process for high-speed, low-cost production. The next step is to establish if local stitch removal patterns can be created for multi-ply preforms. Theoretically, this should be possible, but the number of optimisation variables will increase

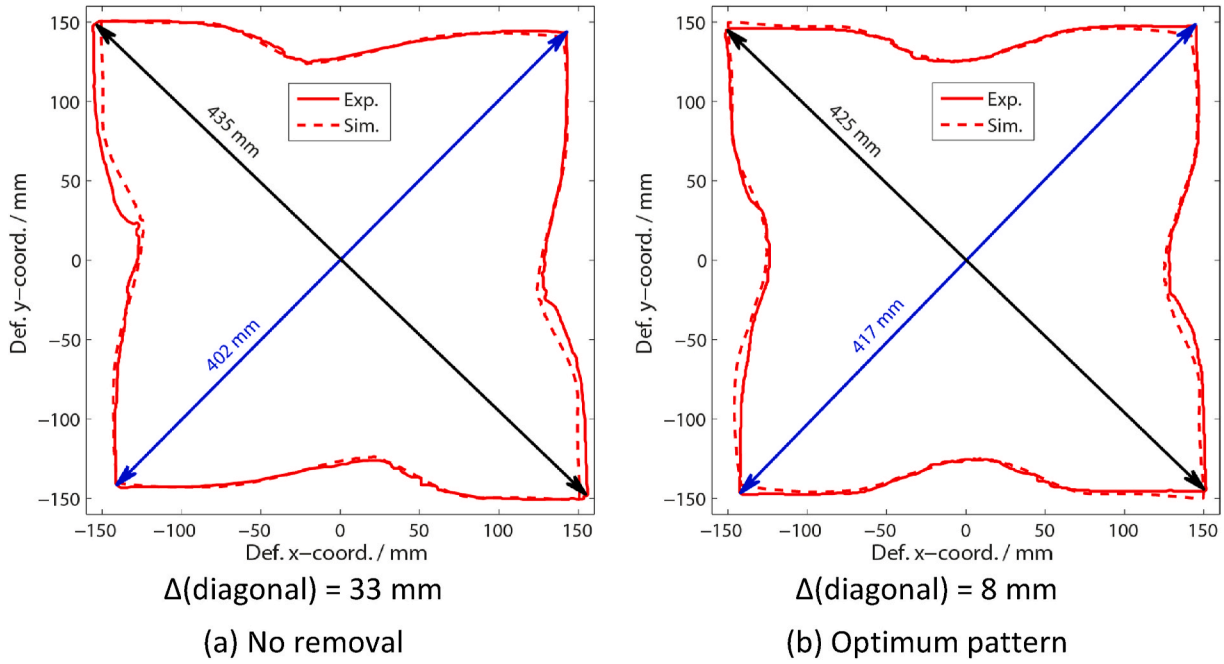

Fig. 16. Predicted perimeter shapes of the preforms from simulations compared against experiments. (Perimeters are taken from the concave images in Fig. 12). (a) No removal (b) Optimum pattern

significantly due to the increase in fabric surface area, and therefore it may no longer be appropriate to directly use the binary encoding scheme. There are two potential solutions: (1) Optimise each ply individually using the developed methodology presented here to provide a starting point for the optimisation of the stacked plies. Then conduct a near optimisation for the whole stack, which will require significantly less computation time. (2) Use coarse division of each ply to identify potential regions for stitch removal, and then optimise the stitch removal pattern according to finer divisions within these sub-regions.

Declaration of competing interest

The authors declare that they have no known competing financial interests or personal relationships that could have appeared to influence the work reported in this paper.

Acknowledgements

This work was funded by the Engineering and Physical Science Research Council [Grant number: EP/P006701/1], as part of the "EPSRC Future Composites Manufacturing Research Hub".

Appendix A. Fabric model and implementation

A hypo-elastic non-orthogonal constitutive model [24,38,39] was employed for the NCF to track the in-plane fibre direction during forming. In the user-defined VUMAT subroutine, the strain increment is supplied by Abaqus/Explicit in the Green-Naghdi (GN) coordinate frame at each time increment. The GN base vectors in the initial configuration, ${}^{0}\mathbf{g}_{\alpha}$ ($\alpha = 1, 2, 3$), can be updated using the rotation tensor $\mathbf{R}$ obtained from the polar decomposition of the deformation gradient $\mathbf{F}$ as

$$\mathbf{R} = \mathbf{F}\mathbf{U}^{-1} \tag{A. 1}$$

$$\mathbf{g}_{\alpha} = \mathbf{R}.{}^{0}\mathbf{g}_{\alpha} \tag{A. 2}$$

where $\mathbf{U}$ is the right stretch tensor.

The current fibre directions, $\mathbf{e}_{fi}$ (i=1, 2), are determined using $\mathbf{F}$ as

$$\mathbf{e}_{fi} = \frac{\mathbf{F}.{}^{0}\mathbf{e}_{fi}}{\left\|\mathbf{F}.{}^{0}\mathbf{e}_{fi}\right\|} \tag{A. 3}$$

where ${}^{0}\mathbf{e}_{fi}$ denote the initial fibre directions.

The corresponding contravariant vectors of $\mathbf{e}_{fi}$ (i=1, 2) are

$$\mathbf{e}^{fi} = \frac{\mathbf{e}_{fi} - \left(\mathbf{e}_{fi}\cdot\mathbf{e}_{fj}\right)\cdot\mathbf{e}_{fj}}{\left\|\mathbf{e}_{fi} - \left(\mathbf{e}_{fi}\cdot\mathbf{e}_{fj}\right)\cdot\mathbf{e}_{fj}\right\|} \quad \left(j = 1, 2;\ i \neq j\right) \tag{A. 4}$$

The normal vectors of the fabric surface are determined as

$$\mathbf{e}_{f_3} = \mathbf{e}^{f_3} = \frac{\mathbf{e}_{f_1} \times \mathbf{e}^{f_2}}{\left\|\mathbf{e}_{f_1} \times \mathbf{e}^{f_2}\right\|} = \frac{\mathbf{e}^{f_1} \times \mathbf{e}_{f_2}}{\left\|\mathbf{e}^{f_1} \times \mathbf{e}_{f_2}\right\|} \tag{A. 5}$$

Consequently, the current fibre coordinate frames corresponding to $\mathbf{e}_{f_1}$ and $\mathbf{e}_{f_2}$ are established based on two sets of base vectors, i.e. $[\mathbf{e}_{f_1}, \mathbf{e}^{f_2}, \mathbf{e}^{f_3}]$ and $[\mathbf{e}^{f_1}, \mathbf{e}_{f_2}, \mathbf{e}^{f_3}]$ respectively. The transformation matrices between the GN coordinate frame and the fibre coordinate frames are

$$\mathbf{Q}_{f_1} = \mathbf{Q}_{f_1 \to \mathrm{GN}} = \begin{bmatrix} \mathbf{g}_1 \cdot \mathbf{e}_{f_1} & \mathbf{g}_1 \cdot \mathbf{e}^{f_2} & \mathbf{g}_1 \cdot \mathbf{e}^{f_3} \\ \mathbf{g}_2 \cdot \mathbf{e}_{f_1} & \mathbf{g}_2 \cdot \mathbf{e}^{f_2} & \mathbf{g}_2 \cdot \mathbf{e}^{f_3} \\ \mathbf{g}_3 \cdot \mathbf{e}_{f_1} & \mathbf{g}_3 \cdot \mathbf{e}^{f_2} & \mathbf{g}_3 \cdot \mathbf{e}^{f_3} \end{bmatrix} \tag{A. 6}$$

$$\mathbf{Q}_{f_2} = \mathbf{Q}_{f_2 \to \mathrm{GN}} = \begin{bmatrix} \mathbf{g}_1 \cdot \mathbf{e}^{f_1} & \mathbf{g}_1 \cdot \mathbf{e}_{f_2} & \mathbf{g}_1 \cdot \mathbf{e}^{f_3} \\ \mathbf{g}_2 \cdot \mathbf{e}^{f_1} & \mathbf{g}_2 \cdot \mathbf{e}_{f_2} & \mathbf{g}_2 \cdot \mathbf{e}^{f_3} \\ \mathbf{g}_3 \cdot \mathbf{e}^{f_1} & \mathbf{g}_3 \cdot \mathbf{e}_{f_2} & \mathbf{g}_3 \cdot \mathbf{e}^{f_3} \end{bmatrix} \tag{A. 7}$$

The strain increment in the GN coordinate frame, $d\boldsymbol{\varepsilon}_{\mathrm{GN}}$ can be transformed to the fibre coordinate frames

$$d\boldsymbol{\varepsilon}_{f_i} = \mathbf{Q}_{f_i}^T \cdot d\boldsymbol{\varepsilon}_{\mathrm{GN}} \cdot \mathbf{Q}_{f_i} \tag{A. 8}$$

Thus, stress increments in the fibre frames can be computed using the corresponding strain increments

$$d\boldsymbol{\sigma}_{f_i} = \mathbf{C}_{f_i} : d\boldsymbol{\varepsilon}_{f_i} \cdot \tag{A. 9}$$

where $\mathbf{C}_{f_i}$ is the constitutive tensor in the ith fibre direction. The explicit forms of Eq. (A. 9) can be determined for the two fibres by assuming the elastic moduli in the fibre directions and the shear modulus are the only non-zero values:

$$\begin{bmatrix} d\sigma_{11} \\ d\sigma_{22} \\ d\sigma_{12} \end{bmatrix}_{f_1} = \begin{bmatrix} E_{f_1} & 0 & 0 \\ 0 & 0 & 0 \\ 0 & 0 & G_{12}(\gamma) \end{bmatrix} \begin{bmatrix} d\varepsilon_{11} \\ d\varepsilon_{22} \\ d\varepsilon_{12} \end{bmatrix}_{f_1} \tag{A. 10}$$

$$\begin{bmatrix} d\sigma_{11} \\ d\sigma_{22} \\ d\sigma_{12} \end{bmatrix}_{f_2} = \begin{bmatrix} 0 & 0 & 0 \\ 0 & E_{f_2} & 0 \\ 0 & 0 & G_{12}(\gamma) \end{bmatrix} \begin{bmatrix} d\varepsilon_{11} \\ d\varepsilon_{22} \\ d\varepsilon_{12} \end{bmatrix}_{f_2} \tag{A. 11}$$

where, γ is the shear angle ($\gamma = 2\varepsilon_{12}$). It is assumed that the contribution from each yarn to the fabric shear force is equal, therefore $G_{12}(\gamma)$ can be determined from the normalised shear force (F_{norm}) in Table 1:

$$G_{12}(\gamma) = \frac{F_{\mathrm{norm}}(\gamma)}{t_{\mathrm{NCF}}} \cdot \frac{L_{\mathrm{NCF}}}{L_{\mathrm{frame}}} \tag{A. 12}$$

where, t_{NCF} is the thickness of each biaxial NCF ply, L_{NCF} is the length of the central region of shear deformation in the picture frame shear test, L_{frame} is the edge length of the picture frame.

The stress tensor in each fibre coordinate frame at the end of each time increment ($\boldsymbol{\sigma}_{f_i}^{\mathrm{new}}$) is updated by

$$\boldsymbol{\sigma}_{f_i}^{\mathrm{new}} = \boldsymbol{\sigma}_{f_i}^{\mathrm{old}} + d\boldsymbol{\sigma}_{f_i} \left(\mathrm{i} = 1,\ 2\right) \tag{A. 13}$$

where $\boldsymbol{\sigma}_{f_i}^{old}$ is the stress tensor at the beginning of each time increment.

Finally, the stress tensors in both fibre coordinate frames are transformed back to the GN frame and superimposed for updating the stress tensor at each integration point.

$$\boldsymbol{\sigma}_{\mathrm{GN}}^{\mathrm{new}} = \mathbf{Q}_{f_1} \cdot \boldsymbol{\sigma}_{f_1}^{\mathrm{new}} \cdot \mathbf{Q}_{f_1}^T + \mathbf{Q}_{f_2} \cdot \boldsymbol{\sigma}_{f_2}^{\mathrm{new}} \cdot \mathbf{Q}_{f_2}^T \tag{A. 14}$$

This value is returned to Abaqus/Explicit from the VUMAT. This loop will be repeated until the end of the forming simulation.

Appendix B. Workflow of Matlab GA Toolbox

Matlab provides a GA Toolbox that was employed to optimise the intra-ply stitch removal pattern. The workflow of this toolbox is as follows [2,40]:

Step 1. Create a random initial population to start the optimisation process.

Step 2. Generate new populations. In each loop, called a "generation", the GA algorithm assesses the fitness score for every individual in the current generation and then creates the next population accordingly. In each loop, the new population is created according to the following steps:

(a) Calculate the fitness score for every individual in the current population using the defined fitness function - the so-called raw fitness score.
(b) Convert the raw fitness scores into a useable range of values (expectation values) by scaling.
(c) Select individuals as "parents", based on their expectation.
(d) Rank the individuals in the current population and choose the individuals with lower fitness scores, called "elites", which are passed to the next population.

(e) Produce children from the parents by either mutations (i.e. making random changes to a single parent) or crossovers (i.e. combining the vector entries of a pair of parents).
(f) Update the current population with the children as the next generation.

Step 3. Repeat Step 2 until one of the GA stopping criteria is met.

References

[1] Huebner M, Diestel O, Sennewald C, Gereke T, Cherif C. Simulation of the drapability of textile semi-finished products with gradient-drapability characteristics by varying the fabric weave. Fibres Text East Eur 2012;5(94):88–93.
[2] Chen S, Endruweit A, Harper L, Warrior N. Inter-ply stitching optimisation of highly drapeable multi-ply preforms. Compos Appl Sci Manuf 2015;71:144–56.
[3] Molnar P, Ogale A, Lahr R, Mitschang P. Influence of drapability by using stitching technology to reduce fabric deformation and shear during thermoforming. Compos Sci Technol 2007;67(15):3386–93.
[4] Duhovic M, Mitschang P, Bhattacharyya D. Modelling approach for the prediction of stitch influence during woven fabric draping. Compos Appl Sci Manuf 2011;42(8):968–78.
[5] Chen S, McGregor O, Endruweit A, Elsmore M, De Focatiis D, Harper L, Warrior N. Double diaphragm forming simulation for complex composite structures. Compos Appl Sci Manuf 2017;95:346–58.
[6] Alshahrani H, Hojjati M. Experimental and numerical investigations on formability of out-of-autoclave thermoset prepreg using a double diaphragm process. Compos Appl Sci Manuf 2017;101:199–214.
[7] Chen S, McGregor O, Endruweit A, Harper L, Warrior N. Simulation of the forming process for curved composite sandwich panels. Int J Material Form 2019:1–14.
[8] Chen S, McGregor O, Endruweit A, Harper L, Warrior N. Finite element forming simulation of complex composite sandwich panels. ICCM22 2019;2019:4107.
[9] Yu W-R, Harrison P, Long A. Finite element forming simulation for non-crimp fabrics using a non-orthogonal constitutive equation. Compos Appl Sci Manuf 2005;36(8):1079–93.
[10] Trochu F, Hammami A, Benoit Y. Prediction of fibre orientation and net shape definition of complex composite parts. Compos Appl Sci Manuf 1996;27(4):319–28.
[11] Turk MA, Vermes B, Thompson AJ, Belnoue JP-H, Hallett SR, Ivanov DS. Mitigating forming defects by local modification of dry preforms. Compos Appl Sci Manuf 2020;128:105643.
[12] Chen S, Harper LT, Endruweit A, Warrior NA. Optimisation of forming process for highly drapeable fabrics. In: 20th international conference on composite materials; 2015. Copenhagen Denmark.
[13] Rashidi A, Milani A. Passive control of wrinkles in woven fabric preforms using a geometrical modification of blank holders. Compos Appl Sci Manuf 2018;105:300–9.
[14] Wang Z, Xie H, Luo Q, Li Q, Sun G. Optimizaition for formability of plain woven carbon fiber fabrics. Int J Mech Sci 2021:106318.
[15] Lin H, Wang J, Long A, Clifford M, Harrison P. Predictive modelling for optimization of textile composite forming. Compos Sci Technol 2007;67(15):3242–52.
[16] Long A, Skordos AA, Harrison P, Clifford M, Sutcliffe MP. Optimisation of sheet forming for textile composites using variable peripheral pressure. Paris, France: SAMPE; 2006.
[17] Chen S, Harper L, Endruweit A, Warrior N. Formability optimisation of fabric preforms by controlling material draw-in through in-plane constraints. Compos Appl Sci Manuf 2015;76:10–9.
[18] Kärger L, Galkin S, Zimmerling C, Dörr D, Linden J, Oeckerath A, Wolf K. Forming optimisation embedded in a CAE chain to assess and enhance the structural performance of composite components. Compos Struct 2018;192:143–52.
[19] Pfrommer J, Zimmerling C, Liu J, Kärger L, Henning F, Beyerer J. Optimisation of manufacturing process parameters using deep neural networks as surrogate models. Procedia CiRP 2018;72:426–31.
[20] Zimmerling C, Pfrommer J, Liu J, Beyerer J, Henning F, Kärger L. Application and evaluation of meta-model assisted optimisation strategies for gripper-assisted fabric draping in composite manufacturing. In: 18th European conference on composite materials (ECCM 2018), athen, GR, june; 2018. 24-28, 2018.
[21] Chen S, McGregor O, Harper L, Endruweit A, Warrior N. Optimisation of local in-plane constraining forces in double diaphragm forming. Compos Struct 2018;201:570–81.
[22] Coutandin S, Brandt D, Heinemann P, Ruhland P, Fleischer J. Influence of punch sequence and prediction of wrinkling in textile forming with a multi-punch tool. J Inst Eng Prod 2018;12(6):779–88.
[23] Lomov SV, Truong Chi T, Verpoest I. 11 - mechanical properties of non-crimp fabric (NCF) based composites: stiffness and strength. In: Lomov SV, editor. Non-crimp fabric composites. Woodhead Publishing; 2011. p. 263–88.
[24] Chen S, McGregor O, Harper L, Endruweit A, Warrior N. Defect formation during preforming of a bi-axial non-crimp fabric with a pillar stitch pattern. Compos Appl Sci Manuf 2016;91:156–67.
[25] Boisse P, Huang J, Guzman-Maldonado E. Analysis and modeling of wrinkling in composite forming. J. Composites Sci. 2021;5(3):81.
[26] Yu F, Chen S, Harper L, Warrior N. Simulating the effect of fabric bending stiffness on the wrinkling behaviour of biaxial fabrics during preforming. Compos Appl Sci Manuf 2021;143:106308.
[27] Yu F, Chen S, Viisainen J, Sutcliffe M, Harper L, Warrior N. A macroscale finite element approach for simulating the bending behaviour of biaxial fabrics. Compos Sci Technol 2020;191:108078.
[28] Matveev MY, Endruweit A, De Focatiis DS, Long AC, Warrior NA. A novel criterion for the prediction of meso-scale defects in textile preforming. Compos Struct 2019;226:111263.
[29] Viisainen J, Hosseini A, Sutcliffe M. Experimental investigation, using 3D digital image correlation, into the effect of component geometry on the wrinkling behaviour and the wrinkling mechanisms of a biaxial NCF during preforming. Compos Appl Sci Manuf 2021;142:106248.
[30] McGregor OPL, Chen S, Haper LT, Endruweit A, Warrior NA. Defect characterisation and selective stitch removal in non-crimp fabrics. In: International conference SAMPE Europe. Amiens; 2015.
[31] Struzziero G, Teuwen JJ, Skordos A. Numerical optimisation of thermoset composites manufacturing processes: a review. Compos Appl Sci Manuf 2019;124:105499.
[32] Fengler B, Hrymak A, Kärger L. Multi-objective CoFRP patch optimization with consideration of manufacturing constraints and integrated warpage simulation. Compos Struct 2019;221:110861.
[33] Fengler B, Kärger L, Henning F, Hrymak A. Multi-objective patch optimization with integrated kinematic draping simulation for continuous–discontinuous fiber-reinforced composite structures. J. Composites Sci. 2018;2(2):22.
[34] Zimmerling C, Dörr D, Henning F, Kärger L. A machine learning assisted approach for textile formability assessment and design improvement of composite components. Compos Appl Sci Manuf 2019;124:105459.
[35] Zimmerling C, Poppe C, Kärger L. Estimating optimum process parameters in textile draping of variable Part Geometries-A reinforcement learning approach. Procedia Manufact. 2020;47:847–54.
[36] Zimmerling C, Trippe D, Fengler B, Kärger L. An approach for rapid prediction of textile draping results for variable composite component geometries using deep neural networks. In: AIP conference proceedings. AIP Publishing LLC; 2019.
[37] Yu F, Chen S, Harper L, Warrior N. Double diaphragm forming simulation using a global-to-local modelling strategy for detailed defect detection in large structures. Compos Appl Sci Manuf 2021;147:106457.
[38] Badel P, Gauthier S, Vidal-Sallé E, Boisse P. Rate constitutive equations for computational analyses of textile composite reinforcement mechanical behaviour during forming. Compos Appl Sci Manuf 2009;40(8):997–1007.
[39] Chen S. Fabric forming simulation and process optimisation for composites. University of Nottingham; 2016.
[40] The MathWorks Inc. How the genetic algorithm works, <https://uk.mathworks.com/help/gads/how-the-genetic-algorithm-works.html>. Accessed September 2021.